Multi-Directional Load Cases on Shared Anchors for Arrays of Floating Structures

Manuel Herduin[#1], Christophe Gaudin[#2], Mark J. Cassidy[#3], Conleth O'Loughlin[#4], James Hambleton[*5]

[#]*Centre for Offshore Foundation Systems, The University of Western Australia, Australia*

[*]*Centre for Geotechnical Science and Engineering, The University of Newcastle, Australia*

[1]manuel.herduin@research.uwa.edu.au

[2]christophe.gaudin@uwa.edu.au

[3]mark.cassidy@uwa.edu.au

[4]conleth.oloughlin@uwa.edu.au

[5]james.hambleton@newcastle.edu.au

***Abstract*— Finite element analysis and geotechnical centrifuge tests were carried out to investigate the multi-directional load distribution acting on shared anchors for arrays of floating structures, and to understand its consequences on the anchor behaviour and performance in order to inform geotechnical engineering design. The results show that the capacity of a typical foundation may be reduced by 10% upon application of one multi-directional load episode.**

***Keywords*— offshore floating renewable energy array, foundation, anchor sharing, cost reduction.**

I. Introduction

In an era of escalating energy demand and climate change, securing the supply of low-emission energy is one of the major challenges of our generation. The world's oceans offer a largely untapped resource, with enormous potential for energy solutions. The last decade has seen a tremendous development of technology, notably associated with floating structures to harvest the energy of the wind and waves.

Implementation of commercially viable floating renewables is however currently obstructed by prohibitively high costs, and significant cost reductions are required to facilitate widespread usage of the technology. Foundations, which can contribute up to 35% of the total cost [1], potentially offer considerable saving. Foundations engineering for renewables is currently undertaken based on the knowledge and expertise developed by the oil and gas industry. However, new approaches are required to enable technology transfer from the offshore oil and gas industry [2], changing the focus from large, expensive one-off structures, to smaller, cheaper ocean energy devices integrated into large arrays (or farms).

Several cost reduction strategies are currently investigated at the Centre for Offshore Foundation Systems, in collaboration with several wave energy partners. Most notably these include, anchor sharing, anchor survivability and probabilistic design.

Anchor sharing consists of designing a foundation to anchor multiple floating structures organised in an array, rather than designing a set of anchors for one renewable energy device (Fig. 1). While significant cost savings might be expected from a reduction of the number of foundations, this results in more complex loading conditions on the anchor. Anchor sharing will notably cause cyclic loading on the anchor to alternate in different directions. This multi-directional alternate cyclic load case is not understood in offshore geotechnics, as the state-of-the-art has been defined for floating oil and gas facilities, which are subjected to unidirectional loading.

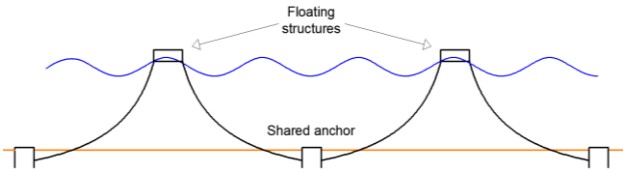

Fig. 1 Application of anchor sharing for two floating structures.

The nature and magnitude of multi-directional loading depends essentially on the hydrodynamics of the floating structure (and its response to varying sea states), the size and shape of the array, the water depth and the type of mooring (either catenary or taut). For floating renewable energy structures, the characteristics of the power take off also affects the magnitude of the loads applied on the foundation. Optimisation of anchor sharing relies on a fundamental understanding of these parameters.

To that purpose, a preliminary study has been undertaken with two distinct objectives: (i) to characterise the variation of load magnitude and direction for a given array configuration, in order to define a potential best load case and worst load case from a foundation engineering perspective and (ii) observe the response of a typical foundation under multi-directional loading to validate the concept of anchor sharing.

In particular, an array of six floating structures was modelled with Sesam DeepC^{TM} software (deepwater floating systems and moorings analysis). A range of linear wave load cases were generated to show the global load responses across the array at each shared anchor point. In parallel, geotechnical centrifuge tests were performed on a reduced scale suction caisson model embedded in sand and subjected to loadings in two different directions.

II. Estimation of Load Distribution on Array of Floating Bodies

A. Analytical framework

The analytical framework presented aims at establishing the loading distribution on a shared anchor, with respect to magnitude and orientation. The case investigated is presented

Proc. of 3rd the Asian Wave & Tidal Energy Conference (AWTEC 2016)
ISBN: 978-981-11-0782-5 :: doi:10.3850/978-981-11-0782-5_13 ::
Published by Research Publishing, Singapore, www.rpsonline.com.sg

in Fig. 2 and consists in two floating bodies A and B connected to five anchors, with one (anchor 3) sharing loads between the two floating bodies, in water depth considered as deep water. A three-point catenary mooring system was chosen for this analysis. The bodies are subjected to a wave series of wavelength λ, at an angle ε with the imaginary line passing through the two floating bodies. W is the inter-device spacing between A and B, $L_{A\text{-}B,\ projected}$ is the projected distance between A and B parallel to the wave direction, α is the angle between the mooring lines (120° for the three-point mooring configuration) and $\Phi_{A\text{-}B}$ is the phase angle representing the time needed by the wave to travel from A to B, along $L_{A\text{-}B,\ projected}$.

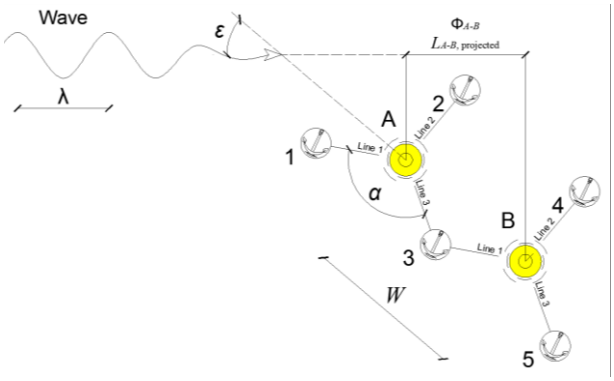

Fig. 2 Top view of two floating bodies (noted A and B) with three-point mooring and one shared anchor point (anchor 3).

Considering the array presented in Fig. 2, the load cases experienced by the two floating bodies are identical, but occur at a different time (this ignores any secondary effects resulting from the wave radiation, second wave order, wake effect or difference in water depth). Consequently the load case of the second body of the array can be established from the load case of the first one, which is then assimilated as the reference load case. A general expression for the force applied on the n^{th} body is

$$F_n = F_{ref} \sin(2\pi f t + \Phi_n) \quad (1)$$

Where F_n and F_{ref} are the forces applied on the set of mooring lines of the n^{th} body and the reference body, respectively, f is the wave frequency, t is the time and Φ_n is the phase angle expressed as:

$$\Phi_n = 2\pi \frac{W \cos(\varepsilon)}{\lambda} \quad (2)$$

The wavelength for deepwater conditions is established from Equation (3):

$$\lambda = \frac{g\, Tp^2}{2\pi} \quad (3)$$

Where g = 9.8 m/s^2 is the gravitational acceleration and Tp is the wave period.

The relation between ε, Φ_n and λ is illustrated in Fig. 3, where λ is plotted against Φ_n/W for six values of ε (0°, 30°, 60°, 70°, 80° and 90°).

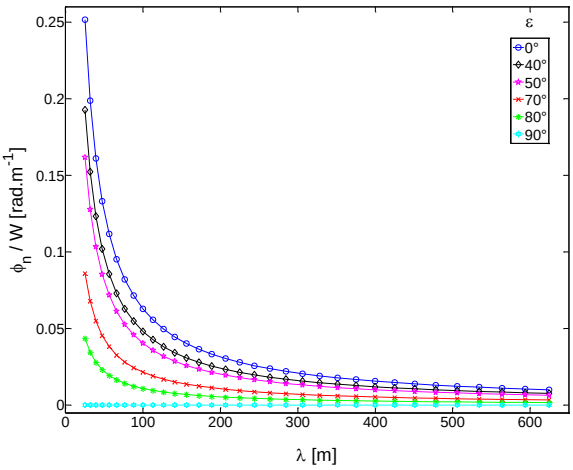

Fig. 3 Functions relating Φ_n/W to the wavelength (λ) for multiple wave directions (ε).

When ε is equal to 90° (e.g. the wave direction is perpendicular to the bodies' alignment), Φ_n/W is constant at zero. However, when ε is equal to 0° (e.g. the wave direction is parallel to the bodies' alignment), Φ_n/W is relatively large at low wavelengths (or wave periods) and rapidly reduces as the wavelength increases.

Focusing on anchor 3, the multi-directional load distribution being experienced by the shared anchor is obtained by the sum of the sinusoidal load signals of each of the two mooring lines connected to the shared anchor. It can be written using the polar coordinates (η_R, α_R), where η_R is the magnitude of the resultant load and α_R is the variation of the angle specifying the direction of the resultant load:

$$\eta_R = \left[F_1{}^2 + F_2{}^2 + 2F_1F_2 \cos(\alpha)\right]^{0.5} \quad (4)$$

$$a_R = \tan^{-1}\left[\frac{F_2 \sin(\alpha)}{F_1 + F_2 \cos(\alpha)}\right] \quad (5)$$

In Equation (4) and (5), F_1 and F_2 are the magnitude of the loads on the two individual mooring lines, and α is the angle between the two mooring lines.

B. Example of application

The analytical framework presented is applied to the three-point mooring system connecting two floating bodies presented in Fig. 2, with a spacing W of 110 m and subjected to a linear wave of period Tp = 6 s (λ = 56 m from Equation (3)) at an angle ε = 40°. The first step is to determine the time series of the loads acting on each of the three mooring lines connected to the floating body A. The load history on the mooring lines is assumed to follow harmonic excitation forces from linear wave theory. In the second step, the phase angle between the two floating bodies is determined from Fig. 3. The three load time series can be transferred from body A to body B with ε = 40°, λ = 56 m and Φ_n/W found from Fig. 3 at 0.08563 rad.m^{-1}. The phase angle $\Phi_{A\text{-}B}$ can then be calculated from equation (2) as $\Phi_{A\text{-}B}$ = (0.08563 rad.m^{-1})(110 m) = 9.42 rad.

This corresponds to a phase angle of π between the two loads, i.e., the two signals are applied one after another on the shared anchor.

The load time series for floating body B can then be deduced from Equation (1) for each of its three mooring lines, as plotted in Fig. 4.

The resulting load magnitude η_R acting on the anchor 3 is determined from Equation (4) as a combination of the load F_1 acting on mooring line 1 of floating body A and the load F_3 acting on mooring line 3 of floating body B. The same procedure is applied to obtain α_R from Equation (5). The computed value of η_R and α_R are presented in Fig. 5. It is noteworthy that (i) the resultant load contains twice as many cycles than the single line loads, but with a magnitude lower than the maximum load on a single line, and (ii) the resultant angle varies significantly between 10° to 110°. Both observations have important consequences with respect to geotechnical behaviour and performance of the anchor.

By varying the wavelength λ and the wave angle ε, it is possible to explore the full range of values of η_R and α_R that are relevant for geotechnical design. The results are presented in Fig. 6. For ε = 40° and Tp = 6 s, corresponding to $\Phi_{A\text{-}B} = \pi$, (i.e. the loads on the two mooring lines acting on anchor 3 are out-of-phase), α_R and η_R exhibit the largest variations, ranging from 1.00 to 1.50 and 10° to 110°, respectively. However, the variation of α_R is lower (ranging from 55° to 82°) for ε = 60° and Tp = 6 s, corresponding to $\Phi_{A\text{-}B}$ = 0 (i.e. the loads on the two mooring lines acting on anchor 3 are in-phase). The same observations can be made if ε is kept constant at 40° and λ varies from 56 m to 84 m.

This corresponds to a variation of the wave period Tp from 6 s to 7.3 s, which is sufficient to modify the load case from out-of-phase to in-phase signals. For the presented case, it is shown that a small variation of the wave direction of 20° or the wave period of 1.3 s is sufficient to change the load distribution from out-of-phase to in-phase loading.

Fig. 6 is important for a geotechnical design perspective. It is unknown at this stage, from the current geotechnical engineering knowledge, whether a highly variable load magnitude (η_R) with limited variation of direction (α_R) is more beneficial than a small variation in magnitude combined with a wide range of direction. This uncertainty needs to be addressed in order to account for geotechnical considerations in the design of arrays of floating bodies and thus to help reduce the cost of foundation engineering.

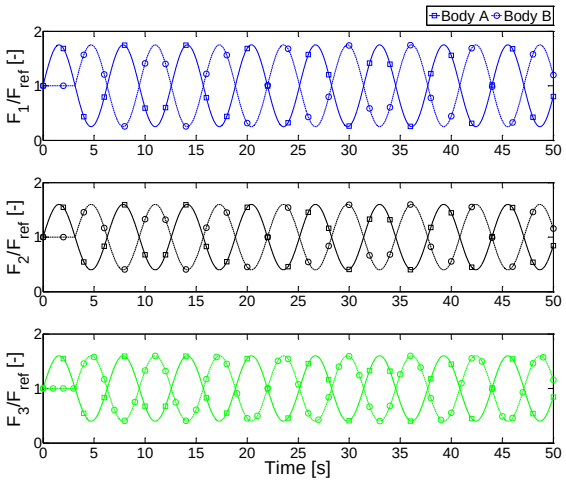

Fig. 4 Time series of the load response at the anchor point for the three lines of the floating body subjected to linear wave.

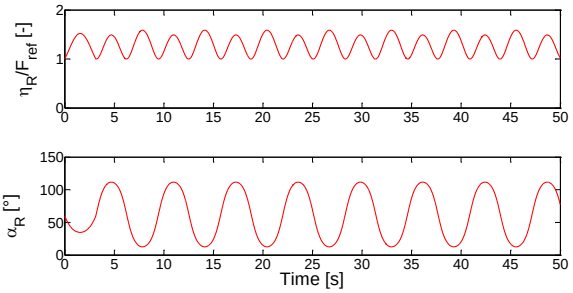

Fig. 5 Time series of the resultant load η_R and the variation of direction α_R.

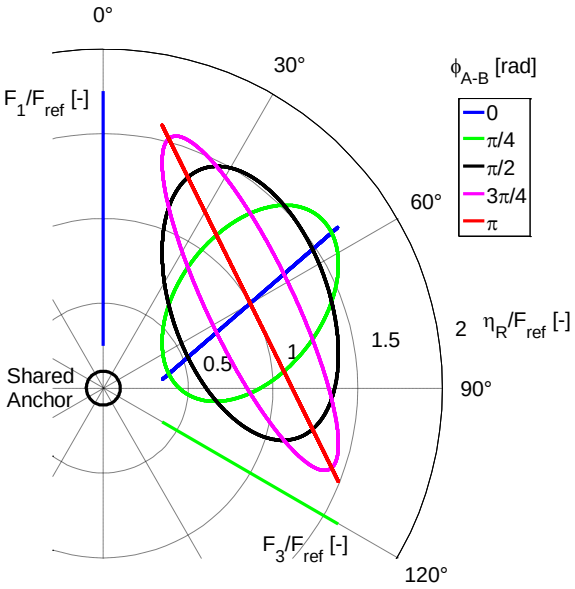

Fig. 6 Load case possibilities for the two load signals F_1 and F_2 with α = 120° and for $\Phi_{A\text{-}B}$ = 0, $\pi/4$, $\pi/2$, $3\pi4$ and π.

III. NUMERICAL MODELLING

The methodology previously described is now applied to an array composed of six floating bodies displayed in a triangular shape (Fig. 7) and subjected to a range of linear waves of varying wavelength or period. The floating bodies are modelled as a generic floating cylinder for simplicity. A total of ten foundations are required to anchor this array with seven anchors sharing loads between floating bodies. In contrast, 18 anchors would be necessary to maintain the six floating bodies in position if loads were not shared between anchors. This triangular pattern has three anchors connected to a single line, six anchors connected to two lines and one anchor connected to three lines.

This exercise ignores hydrodynamic considerations but has sensible assumptions which are described in this section. Its purpose is to generate the potential multi-directional load distribution for a generic floating body triangular array subjected to a range of environmental conditions.

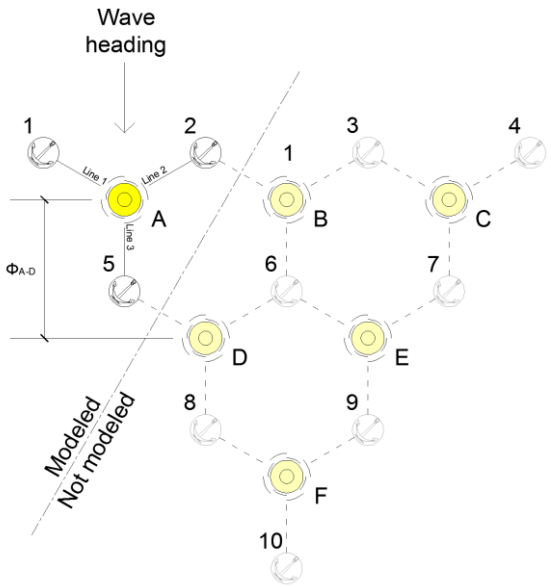

Fig. 7 Top view of the triangular pattern considered.

A. Floating body model and properties

The floating body was created with the sub-package Sesam Genie™. The model was built from plates using guiding geometry, and meshing is generated automatically (Fig. 8). Geometric and hydrodynamics properties of the floating body are given in Table 1.

First-order wave forces acting on the floating bodies were calculated from frequency domain hydrostatic analysis with the hydrodynamic code HydroD™, a sub-package of Sesam. The method used a panel model which calculates the hydrodynamic loads and responses from potential theory and included the forces related to the added mass and potential damping based on Morison's equations. Calculated for 60 angular wave frequencies ranging from 0.22 to 13.2 rad/s, the Response Amplitude Operators were used directly as input for the coupled mooring motion analysis (Sesam DeepC™).

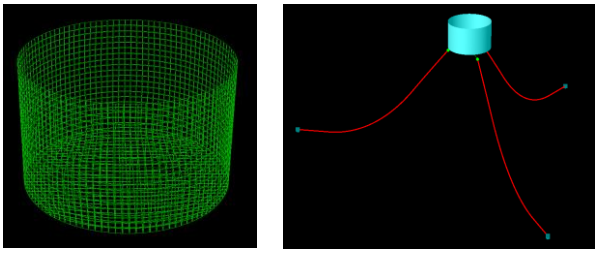

Fig. 8 Finite element representation of the single body (Genie) on the left side and 3D view of the single body (DeepC) on the right side.

TABLE I
GEOMETRIC AND HYDRODYNAMIC PROPERTIES OF THE FLOATING BODY

Diameter, D		16	[m]
Inter-device spacing, L		120	[m]
Height		10	[m]
Volume		2011	[m^3]
Weight		200	[t]
Mass inertia coefficients	I_{xx}	0.0076	
	I_{yy}	0.0076	
	I_{zz}	0.0039	
Added mass coefficients	m_{11}	0.1731	
	m_{22}	0.1731	
	m_{33}	6.8673	

B. Mooring model

The mooring system was made of synthetic ropes and chain segments, with characteristics listed in Table 2. Synthetic fibre ropes are widely used for wave energy devices [3]. The particularity of this type of mooring system is the ability to reduce peak mooring loads through the low variable stiffness of the nylon material. SIMA™ allows a non-linear load-strain distribution as an input. The non-linear axial stiffness profile of the rope was determined from manufacturer data and is provided in Table 3. Chain segments were used at seabed level, for connection with the anchor, as fibre ropes are not abrasion proof.

Drag and added mass coefficients are respectively taken from [4] and [5] without consideration of marine growth. Mooring lines are segmented every 0.5 m for equilibrium calculations.

C. Linear domain analysis

Riflex is a computer programme used by DeepC for the analysis of coupled mooring lines systems and other slender structures. The coupled motion analysis included the calculation of the floating body motion in the time domain simulation with the non-linear effects resulting from the mooring lines. The step by step numerical integration of the dynamic equilibrium equations is based on the Newmark beta method. A time step of 0.01 s was chosen.

TABLE II
MOORING MODEL PROPERTIES

Element		**Nylon rope**	**Stud chain**	
Length		22	55	[m]
Diameter		0.192	0.25	[m]
Weight		0.19	5	[kN/m]
Drag	Cd_n	1.6	2.6	
Coefficient	Cd_a	0	1.4	
Added mass	Ca_n	1	1	
coefficient	Ca_a	1	0	

TABLE III
MOORING STIFFNESS PROPERTIES

Axial force		**Elongation**
[kN]	**[%MBL]***	**[%]**
0	0	0
1442	17.5	8
1648	20	10
2225	27	12
3296	40	13
4779	58	15
4944	60	16
6592	80	18
7004	85	20
8240	100	25

*Minimum Breaking Load

D. Results and discussion

The method presented previously is here applied to obtain η_R and α_R for the fifth anchor of the triangular array as shown in Fig. 7. This anchor is shared by the third line of floating body A and the first line of floating body D.

The results of the numerical simulations are interpreted by plotting the time series of the load response and the motion of the modelled body. Results for Tp = 11 s are presented in this paper from 200 s until 400 s to highlight the steady-state harmonic response of the mooring lines.

Fig. 9 presents the surge, sway and heave motion of the floating body. The floating body experiences a cyclic surge motion of amplitude +/- 0.7 m, which then generates a cyclic variation of the loading angle of the mooring line 1 from the floating body A denoted by α_{A1} within the range of +/- 0.5°. It does not experience sway translation due to the mooring line symmetry with respect to the wave heading.

Fig. 10 presents the load time series on the three mooring lines of the floating body A. The loads on mooring lines 1 and 2 are identical due to the wave heading.

The key results of the numerical analysis are summarised in Fig. 11, which presents the time series of the resultant magnitude η_R and resultant change in loading direction α_R of for shared anchor 5. Note that Fig. 11 was obtained from the analytical framework described previously.

As evident from Fig. 11, the magnitude of η_R is lower than the maximum of the magnitude of F_1, F_3 as the two loads act on the anchor in opposite directions (α = 120°). This is beneficial from a geotechnical design perspective and should be considered in designing array arrangements, acknowledging that this would not be the case for a difference in direction between F_1 and F_3 lower than 90°. The overall benefit of a reduction in the magnitude of the resultant needs however to be balanced with the change in direction of the resultant, which may have detrimental effect on the soil resistance. While α_{D1} (the change in loading direction of the mooring line 1 from the floating body D) oscillates cyclically within the range of one degree and α_{A3} (the change in loading direction of the mooring line three from the floating body A) remains steady, α_R oscillates within a range of +/- 6°. While limited, it is uncertain, whether this may degrade the resistance of the soil.

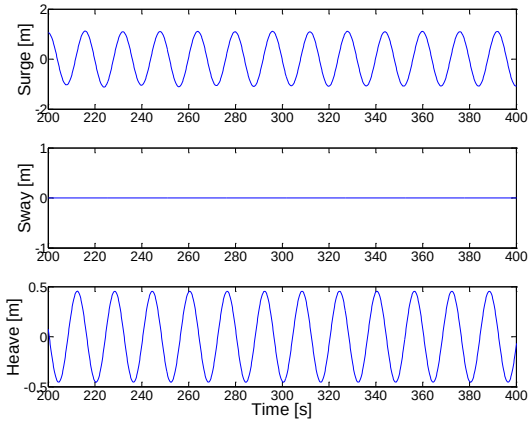

Fig. 9 Motion time series of the floating body.

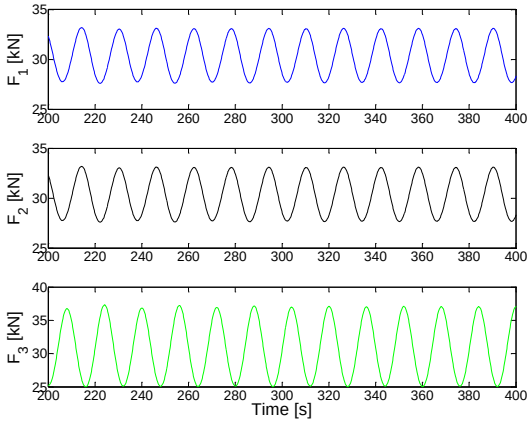

Fig. 10 Load time series on the three mooring lines.

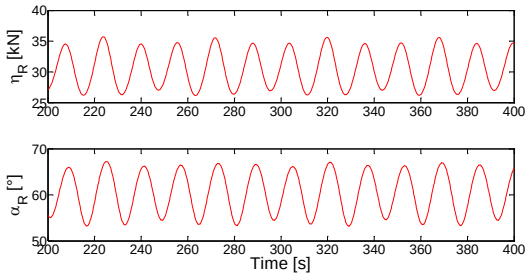

Fig. 11 Time series of the resultant load η_R and angle α_R.

The results discussed above were generalised for varying wave period and Fig. 12 and Fig. 13 present the evolution of η_R and α_R with the non-dimensional wavenumber, respectively. For η_R, only the minimum, mean and maximum values are represented to show the envelope of the resultant load acting on the shared anchor.

Fig. 12 and Fig. 13 are helpful to identify the floating body inter spacing, as a function of the wave period, that would minimise the resultant load magnitude and variation of direction, noting that this ignores any hydrodynamic properties about the performance of the floating energy devices in general, and potential shadow effects in particular.

For $kW < 7$, both η_R and α_R exhibit the maximum values. Increasing the distance between the floating bodies reduces both the magnitude and change in direction of the resultant load, although there is an evident increase in variation of α_R for $kW > 7$.

The analysis is further generalised in Fig. 14, which presents the maximum values of η_R plotted against α_R for all wave periods and for the seven shared anchors of the triangular array. The resultant load is here normalised by the reference load F_{ref} experienced by an anchor connected to one mooring line. This type of graph helps to identify bounds on the multi-directional load cases for each anchor both in term of amplitude and angle. This graph also shows the likelihood of the loading combinations occurring across the array.

Fig. 14 shows a clear difference in loading cases between anchors sharing two mooring lines and anchors sharing three mooring lines. For two mooring lines, the entire multi-directional load case (81% + 5.2% of the global array) is in the range $0 < \alpha_R < 45°$, while the resultant load magnitude never exceeds $1.2F_{ref}$. As mentioned earlier, this multi-directional load case is not well understood on geotechnical engineering. In contrast, for the sixth anchor (with three mooring lines), $\alpha_R = 180°$, indicating that the load case is bi-directional cycling, more common in typical offshore geotechnical engineering. The resultant is obviously lower than the three individual loads, although in this particular case, the individual loads would govern the anchor design.

This numerical approach is based on a linear wave response and further validations with irregular waves are required. However it provided a good introduction to the multi-directional loading problem by showing the important influence of the phase angle Φ_n on the resultant multi-directional load case.

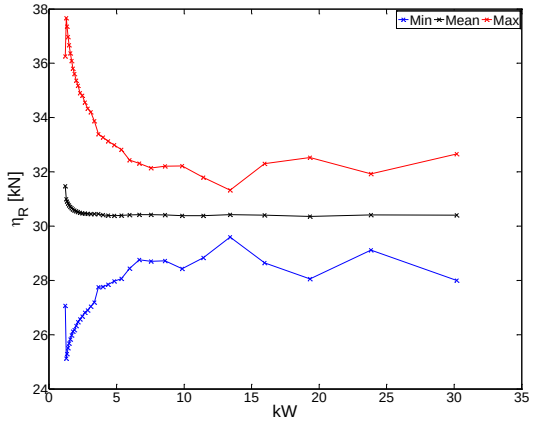

Fig. 12 Resultant load envelope for the range of modelled wave periods.

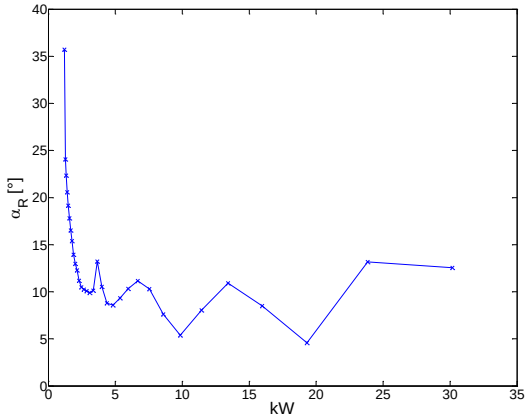

Fig. 13 Resultant angle amplitude for the range of modelled wave periods.

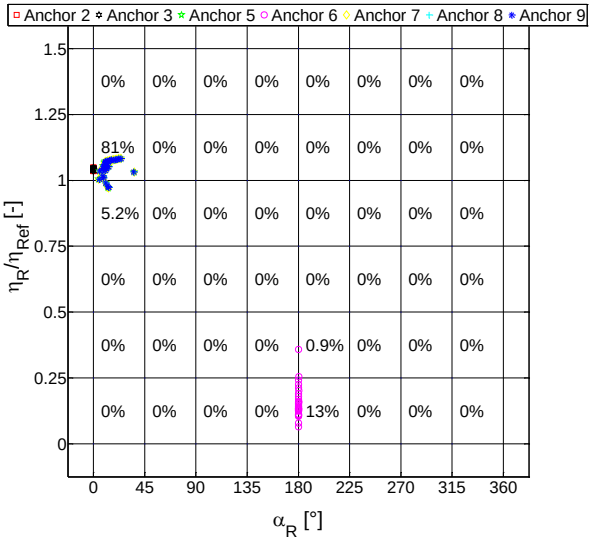

Fig. 14 Summary results of the maximum resultant load amplitude and the variation of direction of the resultant load for the seven shared anchors.

IV. EXPERIMENTAL MODELLING

In order to obtain insights on the effect of multi-directional loading on foundation performance, a preliminary experimental study has been undertaken in the UWA geotechnical centrifuge.

By creating a centrifugal acceleration of *ng*, the centrifuge enables recreation of the same level of geostatic stresses within the soil between the in-situ prototype and a $1/n^{th}$ reduced scale model. The strength and stiffness of soils being dependant of the stress level, this ensures similarity of behaviour between the prototype and the model. In the current experiment, a caisson foundation as shown in Fig. 15 was used for the experiments. Caisson foundations are large diameter steel cylinders, open ended at the bottom and closed at the top, typically 3-30 m long and with an aspect ratio length/diameter (L/D) in the range 1-7. They can be used in clay or sand and have become popular in the last decades due to their ease of installation. For catenary mooring, the mooring line is fixed at a padeye located about one third from the base of the caisson [6].

The purpose of this preliminary experiment was to investigate whether multi-directional loading has an effect on the monotonic bearing capacity of suction caisson in sand. This was performed by applying a load F_1, equal to a fraction of the monotonic capacity, in one direction before loading the caisson to failure in another direction F_2 at an angle α from F_1 (Fig. 15). The load inclination angle β was kept constant at 30° for all tests. Parameters investigated included the magnitude of the first load F_1 and the load angle α.

A. Test programme

The geotechnical centrifuge modelling was performed using the Centre for Offshore Foundation Systems beam centrifuge facility at the University of Western Australia [7]. The test programme is presented in Table 4. A total of 12 tests were performed, three to establish the monotonic capacity and nine to investigate multi-directional loading. Three load angles α = 60°, 90° and 120° were investigated on three samples. The loads investigated along the first loading direction varied from 0.30 to 0.85 times the failure load F_{mono}.

TABLE IV
TEST PROCEDURE

Sample 1	Sample 2	Sample 3
60°	90°	120°
CPT_1	CPT_2	CPT_3
mono_1_1	mono_2_1	mono_3_1
$F1 = 0.30F_{mono}$	$F1 = 0.30F_{mono}$	$F1 = 0.30F_{mono}$
$F1 = 0.50F_{mono}$	$F1 = 0.50F_{mono}$	$F1 = 0.50F_{mono}$
$F1 = 0.85F_{mono}$	$F1 = 0.85F_{mono}$	$F1 = 0.85F_{mono}$

B. Caisson and mooring models

Tests were performed on a 1/100 scale model caisson. The diameter D was 40 mm, and the skirt thickness was 1 mm. The length to diameter ratio was L/D = 1, which is typical for a caisson in sand. The caisson was manufactured from a single piece of aluminium and possessed a smooth surface. Two padeyes were installed at $L/3$ from the tip of the caisson skirt, enabling five combinations of directions of loading, with α = 0°, 60°, 90°, 120° and 180°. The mooring lines were modelled with stainless steel fishing line with 1 mm diameter.

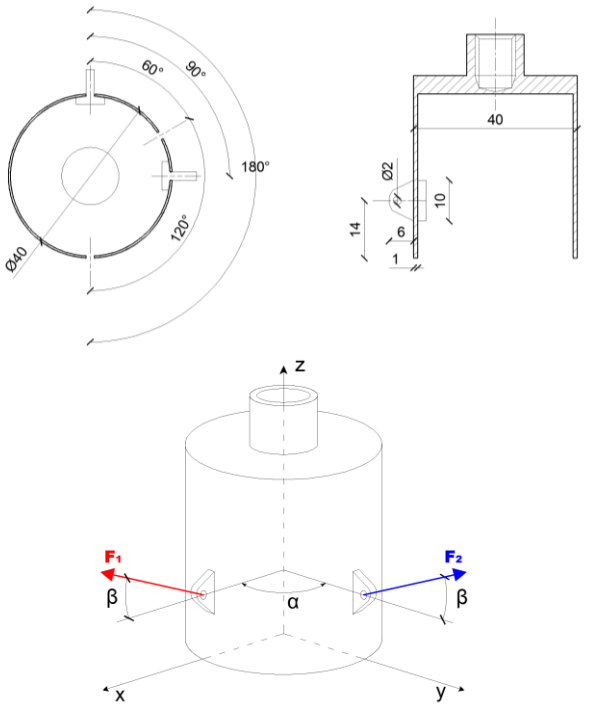

Fig. 15 Model configuration.

C. Soil model

All tests were conducted in dry fine silica sand with relative density D_r > 90%. A Cone Penetration Test (CPT) was performed for each sample to estimate the soil relative density. The physical and mechanical properties of the soil are given in Table 5.

TABLE V
SAND PROPERTIES

Specific gravity, G_s	2.65	
Minimum void ratios, e_{min}	0.49	
Maximum void ratios, e_{max}	0.78	
Minimum dry densities, γ_{min}	14.6	[kN/m^3]
Maximum dry densities, γ_{max}	17.4	[kN/m^3]
Average particle size, D_{50}	0.19	[mm]

D. Test Procedure

The soil samples were reconstituted in a rectangular strongbox, in which five caisson tests were performed.

In each sample, the first two tests aimed at determining the monotonic capacity, and these were followed by three multi-directional tests. **Error! Reference source not found.** shows the experimental setup for α = 120°. Before each test, the caisson was pushed into the sand at earth gravity at a rate of 0.2 mm/s. During testing, the centrifuge was spun at 100 g and the caisson was loaded at a rate of 0.1 mm/s.

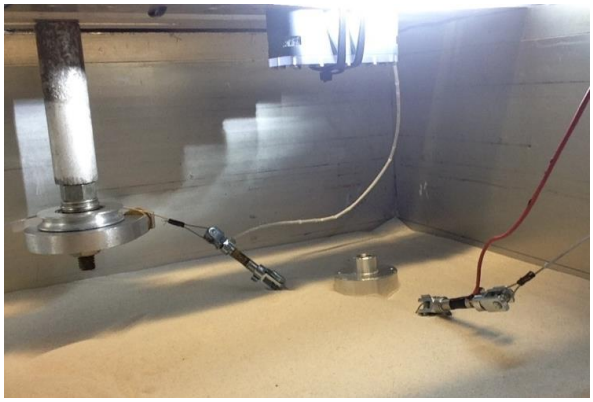

Fig. 16 Experimental setup showing the caisson model in the centrifuge box before testing with α = 120°.

E. Results and discussion

Measured displacements and loads are presented in Fig. 17. The loads are normalised by F_{mono} of the relevant sample and the displacements are normalised by the caisson diameter.

Results are summarised in Fig. 18, which plots the ratio of the failure load measured on the second loading direction, F_2 by the monotonic capacity measured on the first loading direction, F_{mono}. This ratio is denoted by $R_{2\text{-}m}$ and it varies as a function of the initial loading ratio (0.30 $F_{mono,}$ 0.50 $F_{mono,}$ 0.85 F_{mono}) and the direction of loading (α = 60°, 90° and 120°). Fig. 18 indicates the conditions where the capacity of the caisson is increased ($R_{2\text{-}m}$ > 1) or reduced ($R_{2\text{-}m}$ < 1).

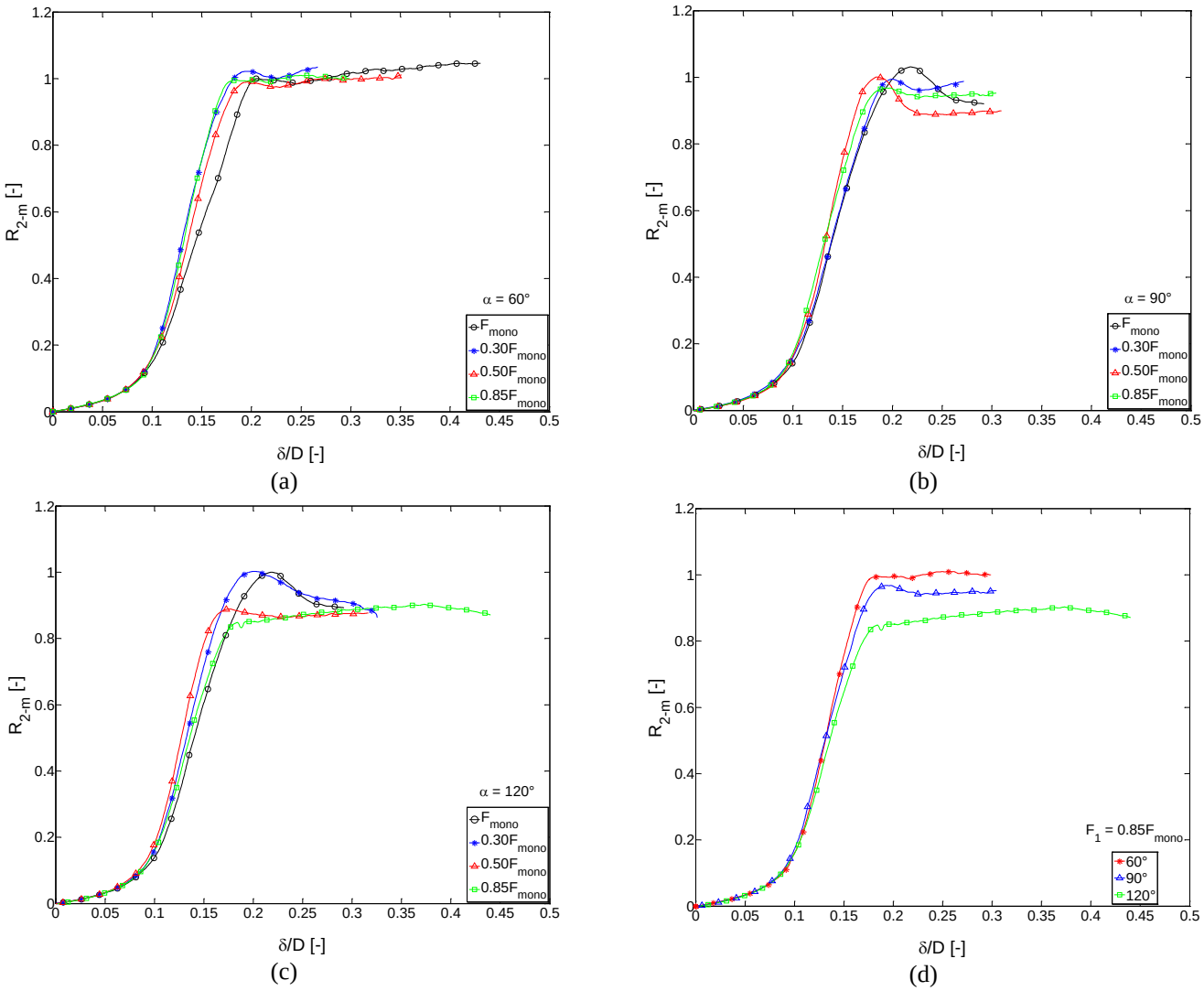

Fig. 17 Measured loads ($R_{2\text{-}m}$) and displacements (δ/D) for multiple values of load angle α. Plots (a), (b) and (c) show results for α = 60°, 90° & 120° respectively. Plot (d) shows the results for all values of α and F_1 = 0.85F_{mono}.

Observations are as follows:

- At low loading levels in the first loading direction (i.e. $F_1 = 0.30F_{mono}$), the capacity of the caisson remains effectively unchanged (i.e. $R_{2\text{-}m} = 1$), regardless of the change in loading direction.
- For a change in loading direction of $\alpha = 60°$, the capacity of the caisson remains unchanged (i.e. $R_{2\text{-}m} = 1$), regardless of the level of loading in the first direction.
- For a change in loading direction of $\alpha = 90°$, the capacity of the caisson is slightly reduced, by about 4%, only for the highest loading ratio.
- It is only for a change in loading direction of $\alpha = 120°$, and for a level of loading in the first direction of 50% or more of the monotonic capacity, that the capacity on the second direction is affected. It is reduced by about 10-11%, with no clear evidence of an increase in reduction with increasing in loading ratio.
- For the highest loading ratio ($F_1/F_{mono} = 0.85$), the capacity of the caisson reduces progressively with increasing change in the loading direction, from 4% at $\alpha = 90°$ to 10% at $\alpha = 120°$.

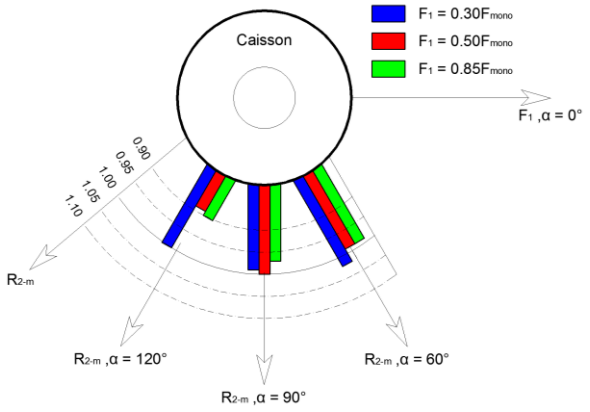

Fig. 18 Summary of centrifuge experimental tests.

Overall, the effect on multi-directional loading on caisson capacity appears to be limited for one episode of multi-directional loading (~10%). It may however be potentially significant over thousands of episodes from repeated wave loading. Preliminary observations also show that the effect of multi-directional loading increases with increasing angle of loading direction, indicating that a low magnitude resultant over a large angle of loading direction might be a more detrimental design scenario than a high magnitude resultant over a small angle of loading direction.

While preliminary, these experimental results clearly indicate that multi-directional loading needs to be carefully accounted for in geotechnical design when considering anchor sharing as a strategy for arrays of floating energy devices.

V. Conclusions

This inter-disciplinary work has provided preliminary insights on the feasibility of anchor sharing concept from a geotechnical engineering perspective.

A theoretical model has been used to investigate the loading regime at the anchor point for an array of floating bodies as a function of the wave period and the spacing of the bodies.

Preliminary calculations have demonstrated that anchor sharing could result in a force resultant acting on the anchor with either (i) a small variation in magnitude combined with a large change of direction or (ii) a large change in magnitude combined with a small change of direction.

To investigate which load case may be the more beneficial for geotechnical design, centrifuge experiments were performed on reduced scale suction caissons in sand. Preliminary results indicated that the first scenario results in potentially significant reduction in caisson capacity. These results need to be validated over a large number of multi-directional loading episodes and for different types of anchor and soil conditions.

Acknowledgments

The study forms part of the activities of the Australian Research Council Centre of Excellence for Geotechnical Science and Engineering and the Lloyd's Register Foundation (LRF) Centre of Excellence.

References

[1] G. Moura Parades, L. Bergdahl, C. Eskilsson and F. Taveira Pinto, "Station keeping design for floating wave energy devices compared to floating offshore oil and gas platforms," in Proc. of 10th European Wave and Tidal Energy Conference, Alborg, Denmark, 2013.

[2] M. Karimirad, K. Koushan, S. D. Weller, J. Hardwick and L. Johanning, "Applicability of offshore mooring and foundation technologies for marine renewable energy (MRE) device arrays," in Renew 2014 - 1st Int. Conf. on Renewable Energies Offshore, Lisbon, Portugal, 2014.

[3] S. D. Weller, L. Johanning, P. Davies and S. J. Banfield, "Synthetic mooring ropes for marine renewable energy applications," Renewable Energy, vol. 83, pp. 1268-1278, 2015.

[4] DNV-OS-E301, "Position Mooring," 2013.

[5] B. Mutlu Sumer and Jorgen Fredsoe, Hydrodynamics around cylindrical structure, World Scientific Publishing Co.Pte. Ltd., 1997.

[6] DNV-RP-E303, Geotechnical Design and Installation of Suction Anchors in Clay, 2005.

[7] M. F. Randolph, R. J. Jewell, K. J. L. Stone and T. A. Brown, "Establishing a new centrifuge facility," Boulder, Colorado, 1991.